## Supporting information

# In situ surface/interface generation on $Cu_2O$ nanostructures toward enhanced electrocatalytic $CO_2$ to ethylene using operando spectroscopy

Fangfang Chang[1], Yongpeng Liu[1], Juncai Wei[1], Lin Yang[1], and Zhengyu Bai*[1]

*Collaborative Innovation Center of Henan Province for Green Manufacturing of Fine Chemicals, Key Laboratory of Green Chemical Media and Reactions, Ministry of Education, School of Chemistry and Chemical Engineering, Henan Normal University, Xinxiang, Henan 453007, China. Email:* baizhengyu2000@163.com

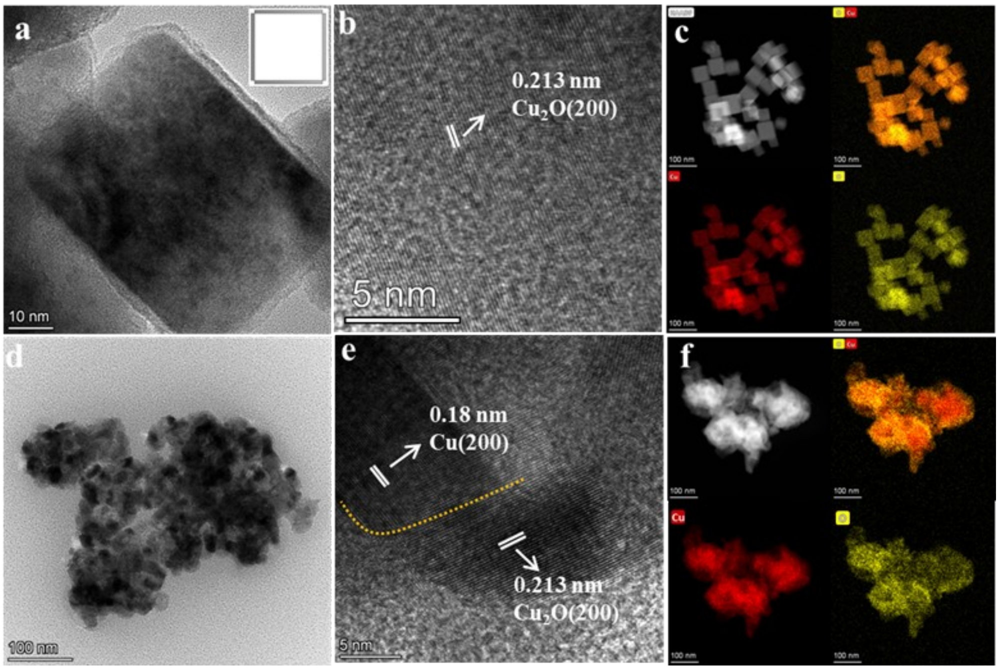


**Fig. S1**. (a) TEM images, (b) HR-TEM, (c) EDS-elemental mapping images of as-synthesized F-$Cu_2O$ catalyst, and (d) TEM images, (e) HR-TEM, (f) EDS-elemental mapping images (Cu species were in red, and O species were in yellow) of surface reconstructed F-$Cu_2O$ samples after reduction at -1.1 V vs. RHE.

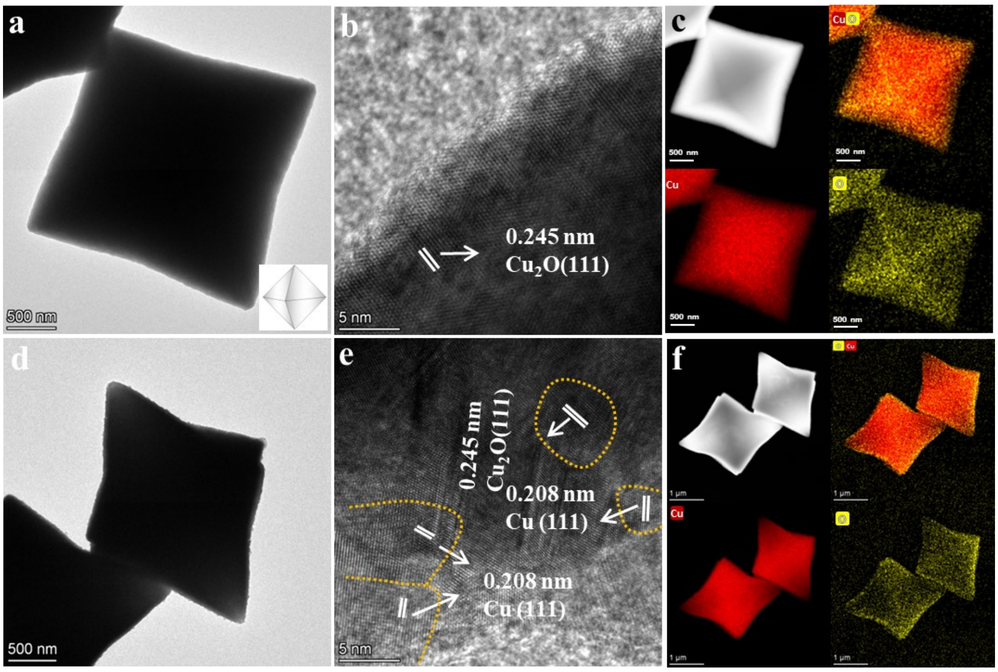


**Fig. S2.** (a) TEM images, (b) HR-TEM, (c) EDS-elemental mapping images of as-synthesized O-$Cu_2O$ catalyst, and (d) TEM images, (e) HR-TEM, (f) EDS-elemental mapping images (Cu species were in red, and O species were in yellow) of surface reconstructed O-$Cu_2O$ samples after reduction at -1.1 V vs. RHE.

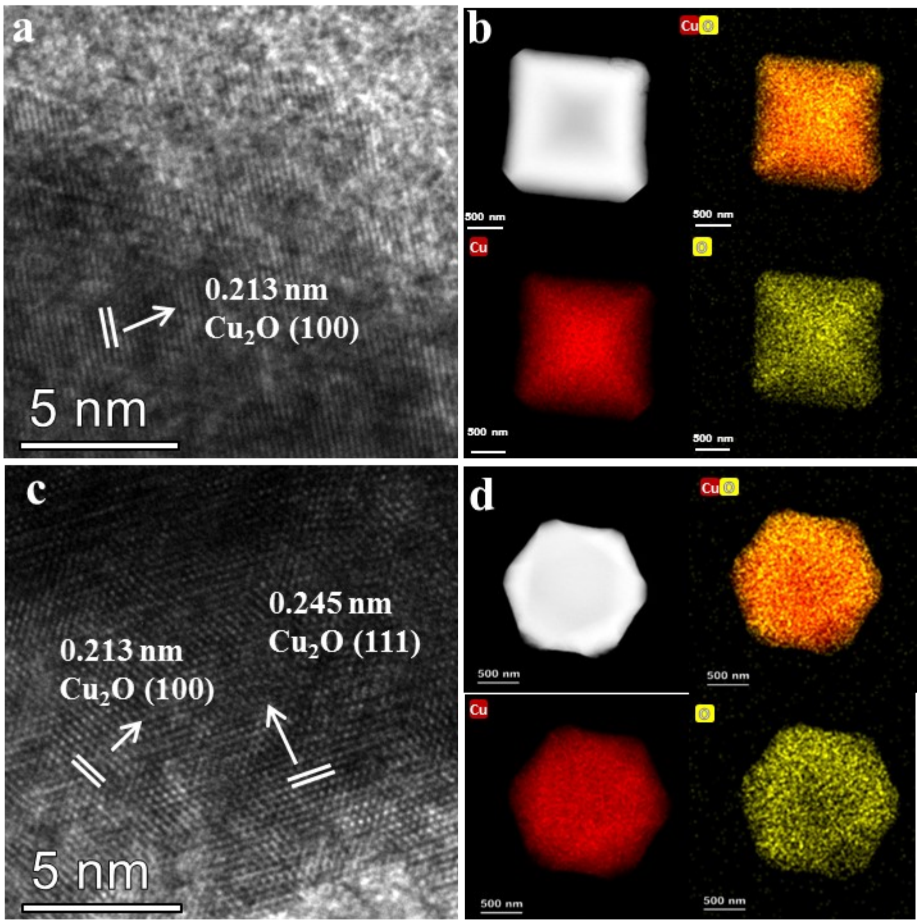


**Fig. S3.** HR-TEM (a, c) and EDS-elemental mapping images (b, and d, Cu species were in red, and O species were in yellow) of the square regions of T-$Cu_2O$ viewed along the (a) [100], (d) [111] directions.

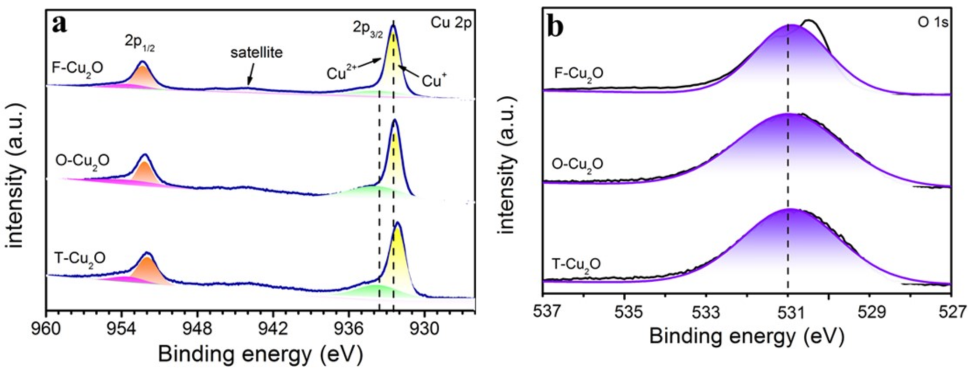


**Fig. S4.** XPS spectra for (a) Cu 2p, (b) O 1s of the three $Cu_2O$ catalysts before $CO_2RR$.

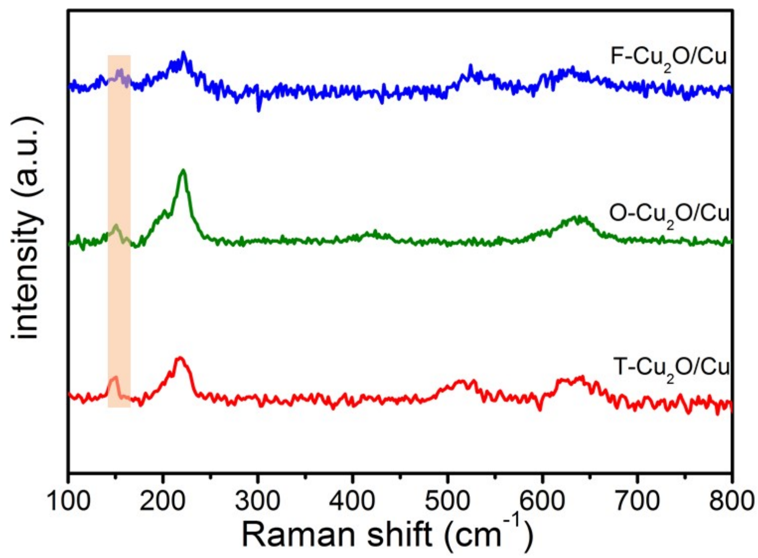


**Fig. S5.** Raman spectra of the three $Cu_2O$ catalysts after reconstruction.

**Table S1.** The content of $Cu^+$ and $Cu^0$ on the surface of the $Cu_2O$ samples after $CO_2RR$ obtained by XPS

| | **Copper species (wt %)** | | |
|---|---|---|---|
| Catalysts | $Cu^+$ | $Cu^0$ | $Cu^+/Cu^0$ |
| F-$Cu_2O$/Cu | 41.6 | 58.4 | 0.71 |
| O-$Cu_2O$/Cu | 36.9 | 63.1 | 0.58 |
| T-$Cu_2O$/Cu | 61.6 | 38.4 | 1.60 |

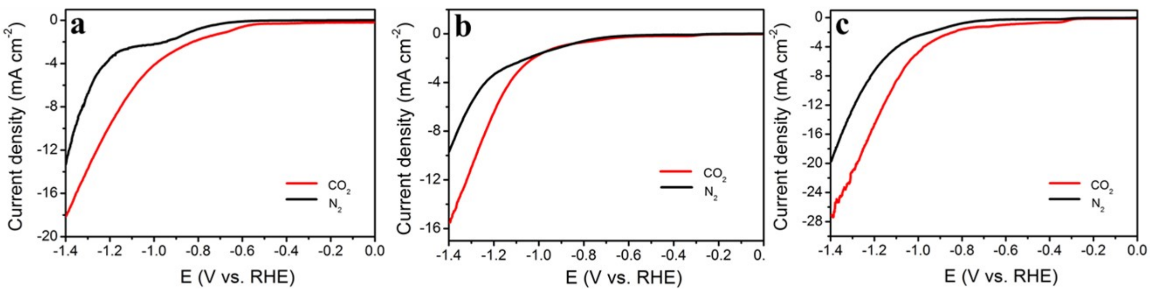


**Fig. S6.** LSV curves of F-$Cu_2O$/Cu (a), O-$Cu_2O$/Cu (b) and T-$Cu_2O$/Cu (c) catalysts in 0.1 M $KHCO_3$ with saturated $N_2$ (black line) and $CO_2$ (red line), respectively, at a 20 mV $s^{-1}$ scan rate.

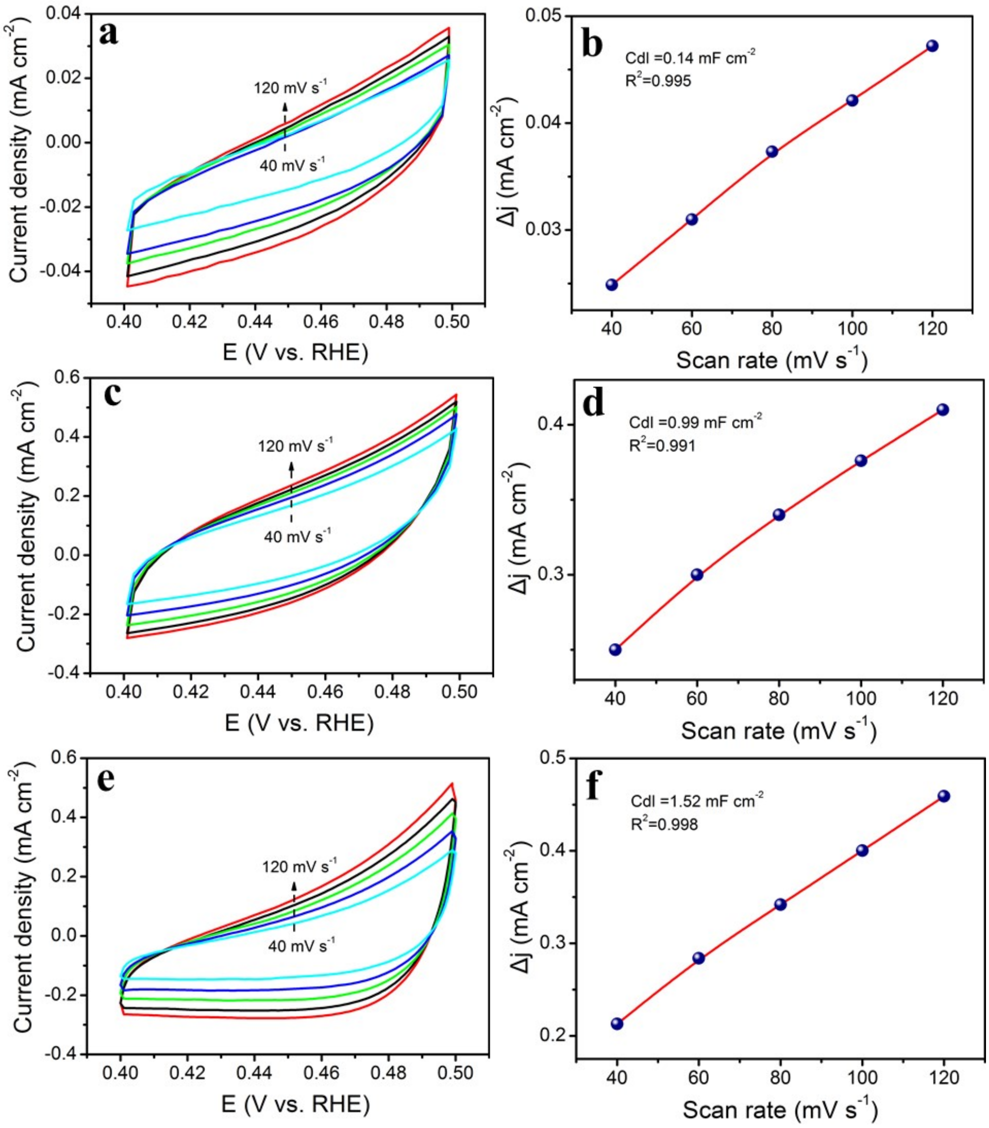


**Fig. S7.** Electrochemical surface area (ECSA) measurement. CVs with various scan rates between 0.4 - 0.5 V vs. RHE in $CO_2$-saturated 0.1 M $KHCO_3$ solution for determining the double-layer capacitance (Cdl) for (a) F-$Cu_2O$/Cu, (c) O-$Cu_2O$/Cu and (e) T-$Cu_2O$/Cu; double layer capacitance of (b) F-$Cu_2O$/Cu, (d) O-$Cu_2O$/Cu and (f) T-$Cu_2O$/Cu.

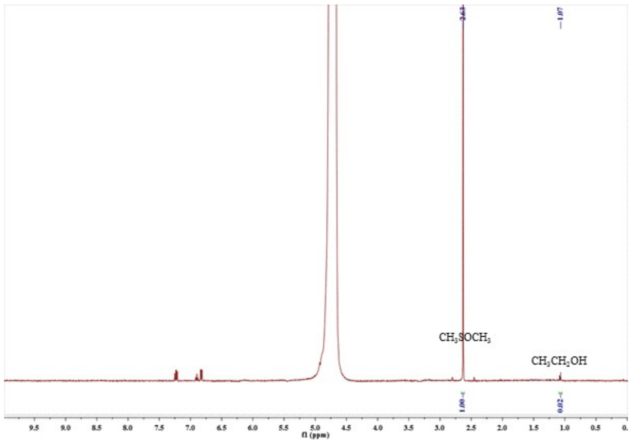


**Fig. S8.** [1]H NMR spectrum of the electrolytes after $CO_2$ reduction.

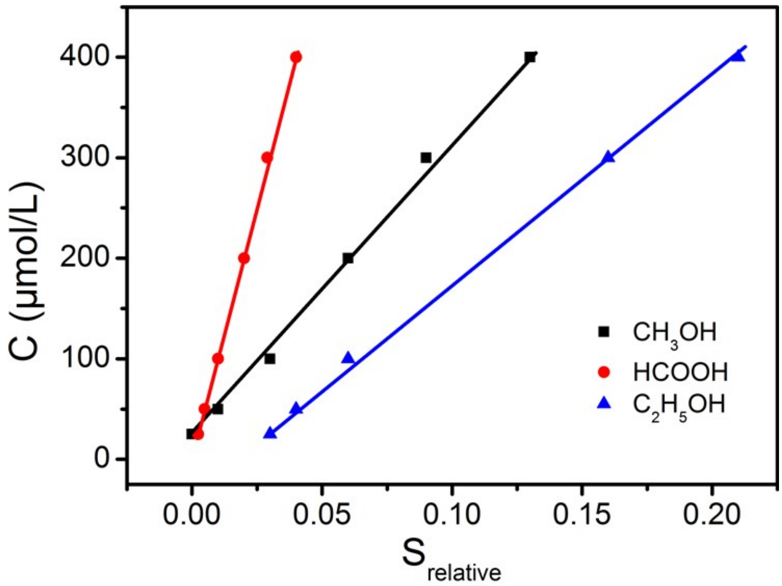


**Fig. S9.** The standard curves of the $CO_2$RR products. The relative peak area (Srelative) is the ratio of the reduction product peak area to the DMSO peak area.

**Table S2.** The linear fitting analytic expressions and variances of the standard curves.

| Expression | C = a + b × Srelative | | |
|---|---|---|---|
| Products | $CH_3CH_2OH$ | $CH_3OH$ | HCOOH |
| Intercept | -27.23 | 21.01 | 0.35 |
| Slope | 2063.95 | 2965.42 | 10086.6 |
| R-Square | 0.993 | 0.996 | 0.999 |

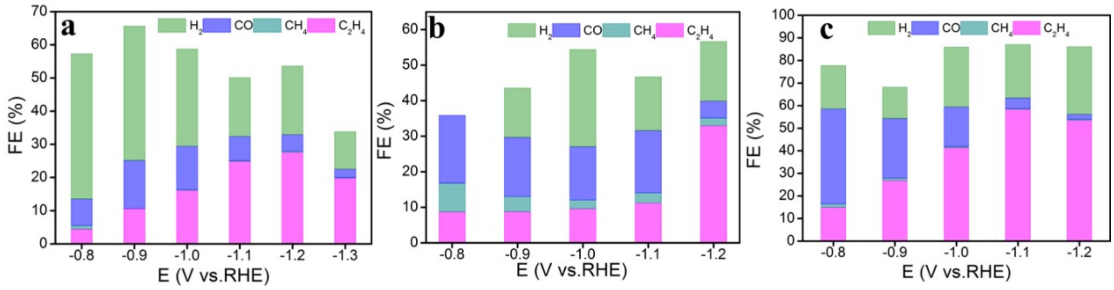


**Fig. S10.** Faradaic efficiencies for $C_2H_4$, CO, $CH_4$ and $H_2$ on (a) F-$Cu_2O$/Cu, (b) O-$Cu_2O$/Cu and (c) T-$Cu_2O$/Cu catalysts at different applied potentials.

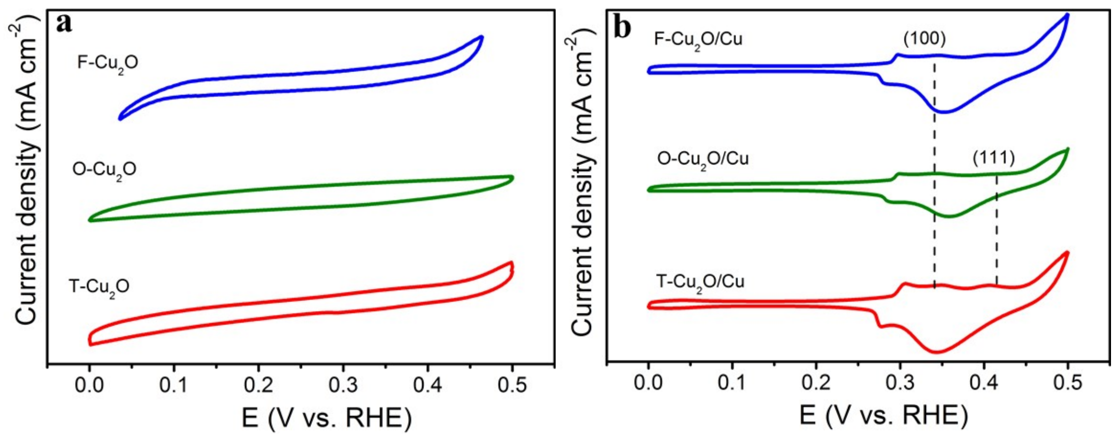


**Fig. S11.** CV curves collected in $N_2$-saturated 1 M KOH for (a) before and (b) after reconstruction $Cu_2O$ catalysts

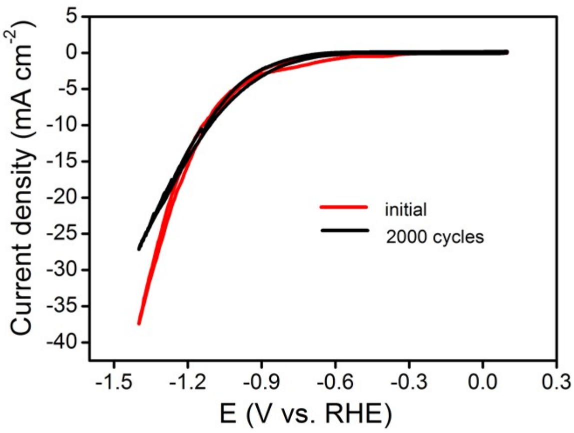


**Fig. S12.** CV curves for T-$Cu_2O$/Cu before and after 2000 potential cycles in 0.1 M $KHCO_3$ solution saturated with $CO_2$ (sweep rate, 50mV/s, potential cycle window: -1.4 and 0 V vs. RHE)

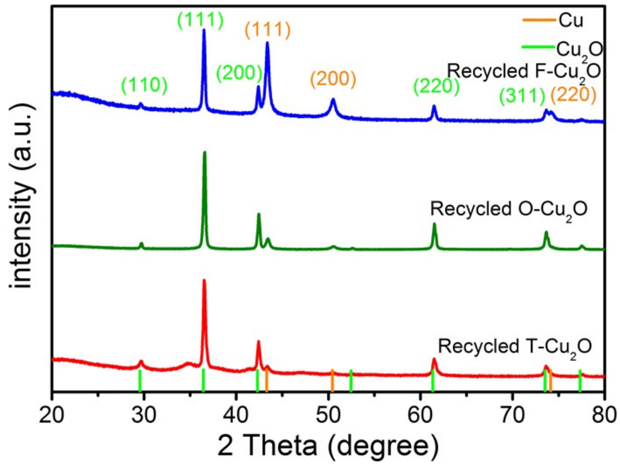


**Fig. S13.** PXRD patterns of the $Cu_2O$ catalysts after CV- Recycled.

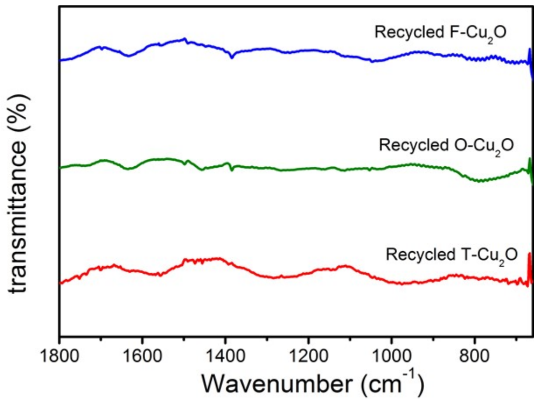


**Fig. S14.** IR spectroscopy of the $Cu_2O$ catalysts after CV- Recycled

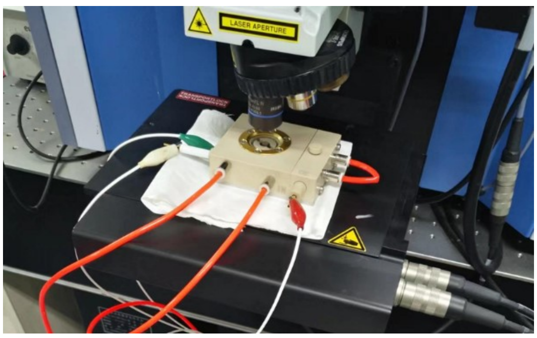


**Fig. S15.** The experimental set up for the in situ Raman spectroscopy measurement.

**Table S3.** Catalytic performances of Cu-based catalysts

| Catalyst | substrate | Electrolyte | $FE_{(C2H4)}$ | E vs. RHE | Ref. |
|---|---|---|---|---|---|
| Cu deposited on $Cu_3N$ | glassy carbon | 0.1 M $KHCO_3$ | 39% | -0.95 V | 1 |
| Cu nanocubes (44 nm) | glassy carbon | 0.1 M $KHCO_3$ | 41.1% | −1.1 V | 2 |
| Fragmentation $Cu_2O$ NPs | glassy carbon | 0.1 M $KHCO_3$ | 57.3% | −1.1 V | 3 |
| Boron-doped copper | glassy carbon | 0.1 M KCl | 52% | −1.1 V | 4 |
| F-modified Cu | GDL | 0.75 M KOH | 65% | −0.89 V | 5 |
| $Cu_2O$-derived Cu NPs | Cu disc | 0.1 M $KHCO_3$ | 32.1% | −1.0 V | 6 |
| Dealloyed Cu–Al | C-GDL | 1 M KOH | 80% | −1.5 V | 7 |
| $Cu_{4.16}CeO_x$ | glassy carbon | 0.1 M $KHCO_3$ | 47.6% | −1.1 V | 8 |
| Hierarchical CuO microboxes | carbon paper | 0.1 M $K_2SO_4$ | 51.3% | −1.05 V | 9 |
| T-$Cu_2O$ | glassy carbon | 0.1 M $KHCO_3$ | 58.0% | −1.1 V | **This work** |

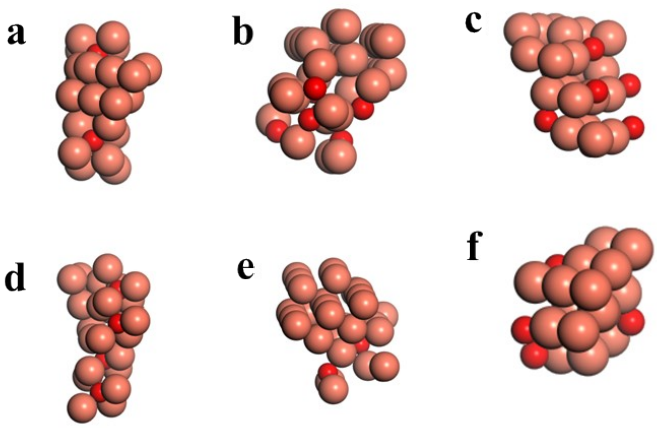


**Fig. S15**. DFT models of (a and d) F-$Cu_2O$/Cu(100), (b and e) O-$Cu_2O$/Cu(111) and T-$Cu_2O$/Cu (111)/(100) interfaces with different view angles.

## Reference


1 Z. Liang, T. Zhuang, A. Seifitokaldani, J. Li, C. Huang, C. Tan, Y. Li, P. De Luna, C. T. Dinh, Y. Hu, Q. Xiao, P. Hsieh, Y. Wang, F. Li, R. Quintero-Bermudez, Y. Zhou, P. Chen, Y. Pang, S. Lo, L. J. Chen, H. Tan, Z. Xu, S. Zhao, D. Sinton, E. Sargent, Copper-on-nitride enhances the stable electrosynthesis of multi-carbon products from $CO_2$, *Nat. Commun.,* 2018, **9**, 3828.

2 A. Loiudice, P. Lobaccaro, E. A. Kamali, T. Thao, B.H. Huang, J. W. Ager, R. Buonsanti, Tailoring copper nanocrystals towards $C_2$ products in electrochemical $CO_2$ reduction, *Angew. Chem. Int. Ed.,* 2016, **55**, 5789–5792.

3 H. Jung, S.Y. Lee, C.W. Lee, M.K. Cho, D.H. Won, C. Kim, H. S. Oh, B. K. Min, Y. J. Hwang, Electrochemical fragmentation of $Cu_2O$ nanoparticles enhancing selective C-C coupling from $CO_2$ reduction reaction, *J. Am. Chem. Soc.,* 2019, **141**, 4624–4633.

4 Y. Zhou, F. Che, M. Liu, C. Zou, Z. Liang, P. De Luna, H. Yuan, J. Li, Z. Wang, H. Xie, H. Li, P. Chen, E. Bladt, R. Quintero-Bermudez, T. Sham, S. Bals, J. Hofkens, D. Sinton, G. Chen, E. Sargent, Dopant-induced electron localization drives $CO_2$ reduction to $C_2$ hydrocarbons, *Nat. Chem.,* 2018, **10**, 974-980.

5 W. Ma, S. Xie, T. Liu, Q. Fan, J. Ye, F. Sun, Z. Jiang, Q. Zhang, J. Cheng, Y. Wang, Electrocatalytic reduction of $CO_2$ to ethylene and ethanol through hydrogen-assisted C–C coupling over fluorine-modified copper, *Nat. Catal.,* 2020, **3**, 478.

6 C. S. Chen, J. H. Wan, B. S. Yeo, Electrochemical reduction of carbon dioxide to ethane using nanostructured $Cu_2O$-derived copper catalyst and palladium (II) chloride, *J. Phys. Chem. C,* 2015, **119**, 26875−26882.

7 M. Zhong, K. Tran, Y. Min, C. Wang, Z. Wang, C. T. Dinh, P. De Luna, Z. Yu, A. S. Rasouli, P. Brodersen, S. Sun, O. Voznyy, C. S. Tan, M. Askerka, F. Che, M. Liu, A. Seifitokaldani, Y. Pang, S.C. Lo, A. Ip, Z. Ulissi, E. H. Sargent, Accelerated discovery of $CO_2$ electrocatalysts using active machine learning. *Nature,* 2020, **581**, 178.

8 D. Wu, C. Dong, D. Wu, J. Fu, H. Liu, S. Hu, Z. Jiang, S. Qiao, X. Du, Cuprous ions embedded in ceria lattice for selective and stable electrochemical reduction of carbon dioxide to ethylene, *J. Mater. Chem. A,* 2018, **6**, 9373-9377.

9 D. Tan, J. Zhang, L. Yao, X. Tan, X. Cheng, Q. Wan, B. Han, L. Zheng, J. Zhang, Multi-shelled CuO microboxes for carbon dioxide reduction to ethylene, *Nano Res.,* 2020, **13**, 768–774.